Evolution of the 2p satellite of Ni nano-clusters on TiO_2(001) surfaces

2008 J. Phys.: Condens. Matter 20 485002

(http://iopscience.iop.org/0953-8984/20/48/485002)

J. Phys.: Condens. Matter **20** (2008) 485002 (7pp) doi:10.1088/0953-8984/20/48/485002

Evolution of the 2p satellite of Ni nano-clusters on TiO_2(001) surfaces

J G Tao[1], J S Pan[2,3], C H A Huan[1,2,3], Z Zhang[2], Y Sun[2], J W Chai[2] and S J Wang[2]

[1] Division of Physics and Applied Physics, School of Physical and Mathematical Sciences, Nanyang Technological University, SPMS-04-01, 21 Nanyang Link, 637371, Singapore
[2] Institute of Materials Research and Engineering, A*STAR (Agency for Science, Technology and Research), 3 Research Link, 117602, Singapore

Received 16 September 2008
Published 17 October 2008
Online at stacks.iop.org/JPhysCM/20/485002

Abstract
Correlation enhancement of electrons in Ni nano-clusters due to confinement in reduced dimensions has been observed. Both the size and shape of the nano-clusters have a strong influence on the Ni 2p satellite structures. For small Ni clusters, apart from the 6 eV satellite, a 3 eV satellite structure emerges in Ni $2p_{3/2}$ photoemission spectra due to the existence of the ^{3}F atomic state. However, the intensity of the 3 eV satellite decreases with increasing cluster size because the Ni 3d level becomes increasingly occupied in large clusters. The increased electron population in the 3d level is achieved through electron transfer from the free-electron-like 4sp states to the unhybridized pure 3d spin down states; the latter is lower in energy than the 3d–4sp hybridized states. The correlation-induced 6 eV satellite energy is enhanced by Ar^+ bombardment. These observations make it feasible to gauge the Ni 3d electron population by probing the 2p photoemission spectra and to modify the supported Ni nano-clusters through thermal treatment and/or ion bombardment.

(Some figures in this article are in colour only in the electronic version)

1. Introduction

In strong correlated systems, the photoemission spectral features become complex and the picture directly related to the density of states (DOS) breaks down. Although nickel metal is an itinerant ferromagnet, it shows localized d band behavior [1] and is therefore an interesting test case to study. A famous example is the Ni 6 eV satellite observed in both core level and valence band photoemission (PE) spectra [2]. Great attention has been paid to the origin of the Ni 6 eV satellite [2–4], its resonant effect [2, 3, 5], and spin-polarization behaviors [2, 6, 7], etc. According to [2], a different screening channel of the core hole induced in the PE process is the origin of the Ni satellite. It can be screened either by d electrons, corresponding to the main peak with a final-state electron configuration of $c^{-1}3d^{10}4s^1$ (where c^{-1} is the core hole), or by s electrons, leading to a 6 eV satellite structure with electron configuration of $c^{-1}3d^94s^2$ in the final state. This mechanism is also valid for valence band satellites. On the other hand, the screening can be performed by electrons in the photoexcited atom (atomic relaxation) as well as by electrons in neighboring atoms (extra-atomic relaxation) [7]. Due to efficient d-wave screening, the extra-atomic relaxation is of importance for Ni satellite structures in x-ray photoelectron spectroscopy (XPS) spectra. The appearance of correlation-induced satellite structures in Ni is also related to the fact that it has a small number of 3d holes (0.6 holes) in the initial state. The d–d hole scattering and the extra-atomic screening of 2p core holes give rise to the satellite features [8].

During the extra-atomic screening of the core hole, the Ni 4sp electrons may transfer to unoccupied states of the 3d level, involving both pure 3d spin down states and unpolarized and hybridized 3d–4sp states [7]. Spin-polarization dependence of the 6 eV satellite suggests that the pure 3d states play a larger role in satellite production than the hybridized 3d–4sp states [9]. The triplet atomic states in Ni satellite features thrive with the transferring of electrons to 3d pure spin down states. Thus the variation of the triplet atomic states in Ni satellite features can be used to trace the electron transfer mechanism when the dimension of Ni nano-clusters is modified because the Ni 3d electron population varies with

[3] Authors to whom any correspondence should be addressed.

scaling the dimension size. Furthermore, correlation-induced satellite structures depend not only on the nature of the d–d electronic interaction but also on additional factors such as the single-particle band structure, the band filling, the weight and center of gravity of the DOS, and the crystal structure [1]. These factors thus introduce some interesting phenomena when any reduced dimension system is considered.

Nano-clusters of metals show different shaped photoemission spectra at the Fermi edge [10] from their bulk counterparts. In the nano-clusters, the surface-to-volume ratio increases enormously. At the surface, the number of neighboring atoms is reduced, leading to a narrower bandwidth and intensified Coulomb correlation energy U within d electrons due to dehybridization of electron wavefunctions. In the end, with stepping down the cluster size, their electronic and/or magnetic natures differ considerably from their bulk counterparts. There are some theoretical predictions on such behaviors [11–13]. Recently, Chen *et al* [12, 13] have predicted that many body effects would be enhanced in a reduced dimensional system based on their calculations. Previously, Binns *et al* [14] reported dimensionally dependent satellite intensity of evaporated vanadium on graphite. As reported in [14], an intense satellite in vanadium 3s core level photoemission was observed when an islanded structure was studied, from which a greater proportion of the signal is from the surface. The continuous film did not even show any satellite signal.

In this paper, we use XPS to explore the enhanced correlation in a reduced dimensional Ni system. The strong influence of the reduced dimensional system on the 3d electron population is verified, hence the electron correlation. The preferred channel for 4sp electrons to replenish the 3d level is predicted when the size of Ni nano-clusters is increased. The enhanced Coulomb correlation energy U intensifies the sp screening of the core hole, which leads to an enhanced satellite strength. The Ni 2p core level spectra show peak asymmetry and satellite positions which are sensitive to the modification upon thermal annealing and Ar^+ ion bombardment.

2. Experimental details

The XPS measurements were performed using a VG ESCALAB 220i-XL instrument (base pressure $<5 \times 10^{-10}$ mbar) equipped with a monochromatic Al Kα (1486.7 eV) x-ray source. The XPS binding energy (BE) was calibrated with pure gold, silver, copper, and Ni standard samples by setting the Au $4f_{7/2}$, Ag $3d_{5/2}$, Cu $2p_{3/2}$ peaks, and Ni Fermi edge at BEs of 83.98 ± 0.02 eV, 368.26 ± 0.02 eV, 932.67 ± 0.02 eV, and 0.00 ± 0.02 eV, respectively. All spectra were recorded in the constant pass energy mode with pass energy of 20 eV and step width of 0.1 eV. Before loading into the chamber, the TiO_2 substrates were cleaned in 10% nitric acid solution and acetone in sequence. Clean TiO_2 surfaces were obtained by repeated cycles of Ar^+ sputtering and ultra high vacuum (UHV) annealing, following the reported recipe [15, 16]. Both the cleanliness and chemical state were verified from high sensitivity and high resolution XPS spectra. Ni was deposited using an Omicron EFM3 e-Beam evaporator in the UHV preparation chamber. The e-beam evaporator deposition rate had been previously calibrated by Rutherford backscattering (RBS) measurements. The desired Ni thickness is achieved through the deposition time, and is also confirmed by *ex situ* cross-section transmission electron microscopy (TEM) measurements. The deposition rate is estimated to be $\sim$0.5 Å min^{-1}.

3. Results and discussion

Figure 1(a) displays the high resolution XPS $2p_{3/2}$ spectra of Ni nano-clusters deposited on $TiO_2(001)$ for 150 s and 900 s, respectively. The main peak (labeled with A) is accompanied by broad satellite features spreading at the higher BE region. The main peak is identified as the $c^{-1}3d^{10}4s^1$ final state, where c^{-1} is the core hole [2]. In small clusters, the modified electronic structure will shift the main peak position to higher BEs [17]. In the present work, we will focus on the evolution of Ni 2p satellite structures with the dimension of the nano-clusters and their origin. To this end, all spectra are normalized and shifted to superimpose the Ni $2p_{3/2}$ main peaks in order to make the comparison easier. The same treatment applies in other figures throughout this paper. After this treatment, the leading edges of the main peaks are identical in shape. The satellite features in the range of 854.0–865.0 eV are characterized as two components, with one at 3.0–4.0 eV higher in BE than the main peak (referred to hereafter as B) and the other one about 6.0 eV higher (referred to hereafter as C or the 6 eV satellite). The satellite features labeled as B and C are indicative of the limitations of one-electron theory [11, 18, 19]. By scanning tunneling microscopy (STM) measurements, the growth of Ni on TiO_2 has been demonstrated to be a Volmer–Weber (cluster growth) mode, forming three-dimensional (3D) clusters even at the lowest coverage [15, 16, 20]. This agrees with the thermodynamic prediction. Based on thermodynamic considerations, the Volmer–Weber growth mode should result when the sum of interfacial energy (γ_i) and surface free energy of the overlayer metal (γ_m) is larger than the surface free energy of the clean substrate (γ_s), i.e.

$$\gamma_i + \gamma_m > \gamma_s \tag{1}$$

and when the sum is less, the film should wet. The surface free energy of Ni (2.34 J m^{-2}) [21] is greater than that of TiO_2 surfaces, which have been calculated to be 1.46 J m^{-2} for the $TiO_2(001)$ surface [22]. On the other hand, there is no chemical reaction between Ni with TiO_2, which leads to a positive value of γ_i [23]. Thus, the left side in equation (1) is always larger than the right side for the Ni/TiO_2 system, resulting in the cluster growth mode. Furthermore, as measured by STM, the size of Ni clusters increases with increasing deposition time, i.e. increasing Ni coverage [15]. The Ni cluster size distribution is controlled by the D/F ratio, where D is the diffusion rate and F is the deposition flux rate [16]. Increasing the D/F ratio will result in a lower cluster density, larger clusters, and a broader size distribution [16]. The size distribution is found to be sharp and approximates a Gaussian distribution [20] or is slightly negatively skewed at room temperature [15], whilst at higher temperature it is slightly positively skewed [15]. Our deposition flux rate and

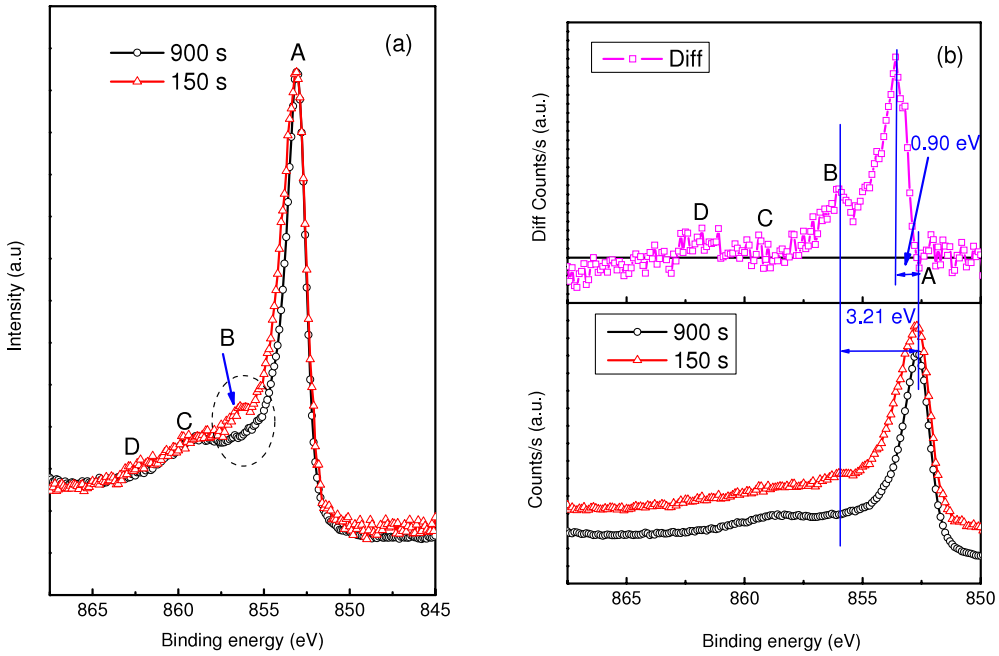

Figure 1. Ni $2p_{3/2}$ XPS spectra for Ni deposited on $TiO_2(001)$ (a), the deposition times are 150 s and 900 s, respectively, specified on the figure. The comparison (lower) and difference (upper) spectra between the 150 s deposited and 900 s deposited are shown in (b). The straight lines are drawn to guide the eye.

other experimental conditions are roughly equivalent to those of Fujikawa's experiments [20], therefore, the size distribution in our experiments would be similar to what they found in [20], which is a sharp approximately Gaussian distribution. Thus, the change of Ni $2p_{3/2}$ spectra in figure 1 can be related to the evolution of the Ni cluster size. As shown in figure 1(a), the B component is robust only for very short deposition time, i.e. small clusters, while the C component does not change evidently. These phenomena are not correlated to the spin–orbit multiplet due to a considerably large separation of the Ni $2p_{1/2}$ peak from $2p_{3/2}$ of the order of 20.0 eV. All the clusters discussed here are in the nanometer (nm) size range with the smallest ones possessing only several atoms [15, 16, 20]. At this size, a strong quantum size effect should occur and the electronic properties are more atomic-like. For Ni atoms in the gas phase, the 2p photoemission spectra consist of many atomic states [19, 24], while the supported atoms are different from the isolated ones [17]. Accompanying the dimensionality increase, the atomic states are becoming overlapped and their weight should be altered. The multiplet complexity of the Ni 2p spectra demonstrated above, especially prominent for smaller clusters, thus originates from the change of electronic properties due to the strong d–d interaction and extra-atomic screening in the reduced dimensional system.

The existence of oxygen atoms in TiO_2 substrate may raise a question as to whether there is any oxidation or not. Hereby, before going into detailed discussion, it is necessary to distinguish the satellite features from the oxide peaks. Despite the fact that there is a small amount of charge transfer between the Ni and TiO_2, the oxidation process (involving mass transport) has been generally ruled out, as discussed in our previous paper [17]. In order to make the present paper self-contained, we briefly summarize the reasons here: (1) the heat of formation ($\Delta_f H^0$) per oxygen atom for TiO_2 (-472 kJ mol^{-1}) is larger than that of NiO (-240.6 kJ mol^{-1}) [25], the interface reaction to form Ni oxide is thus thermodynamically unfavorable; (2) the work function of $TiO_2(001)$ is 2.64 eV [22], much smaller than that of Ni (5.04–5.42 eV) [26], therefore the positive end of the built-in electric field at the Ni and $TiO_2(001)$ interface is pointing from TiO_2 to Ni, which prevents the O^{2-} anion from moving to the Ni side to react [27–29]. The argument is further strengthened below in the discussion of annealing samples.

In Ni, there is a high density of states (DOS) above the Fermi edge (E_F) so that there are many final states into which the electrons can scatter and a reduction of the DOS at E_F leads to weaker satellites [30]. Furthermore, it is concluded that the contribution of empty 4sp bands to a satellite is weak because the scattering of d electrons into sp states has low probability. The intensity of the satellite features is determined by the weight of unoccupied Ni 3d character and by its nature and position above E_F. The Ni 3d characters far above E_F produce a smaller contribution to the d^9 satellites than those just above E_F [30, 31]. The spin momentum is conserved during the photoexcitation process. The minority spin spectrum only contributes to spin triplet final states, whereas the spin singlet final states originate from the majority spin spectrum [32]. Large p–d electrostatic interaction splits the Ni 2p satellites into several atomic states, with assignments of ^{1}D, ^{3}F, ^{3}D, ^{3}P, ^{1}F, and ^{1}P [9, 33]. The peaks at 10.0 eV higher in BE than the Ni $2p_{3/2}$ main peak is attributed to ^{1}F and ^{1}P states of the $2p^5 3d^9$ configuration (labeled as D in figure 1), while they are too weak to be recognized. The well-known 6 eV satellite is attributed to the combination of ^{3}D and ^{3}P states, labeled as C

in figure 1. The ^{1}D and ^{3}F states give rise to the nearest feature to the Ni $2p_{3/2}$ main peak, labeled as B, whose significant weight is governed by the ^{3}F state [32]. In figure 1(a), with increasing the Ni coverage, i.e. increasing the cluster size, the dramatic change of the Ni 2p spectra appears as a reduction of the feature B. The enhanced 3 eV satellite is due to the increase in the d-hole number at the surface [34]. The increase in d-hole number can be associated with the increase in the $3d^8$ configuration in the ground state. On the other hand, since the intensity of feature B is mostly donated by the ^{3}F state, the intensified feature B at low Ni coverage, i.e. smaller cluster size, thus indicates an enhancement of the ^{3}F state. The ^{3}F state is a triplet state caused by pure minority spin down emission. The decreased ^{3}F state with increasing cluster size indicates a reduction of minority 3d hole states, thereby an increased population of 3d minority electron states, in line with the fact that the Ni 3d level is more populated when it goes from atom to bulk.

Furthermore, a direct line-shape comparison of Ni 2p spectra of small clusters (deposition time of 150 s) with large ones (deposition time of 900 s) is displayed in figure 1(b). Their difference spectrum is given in the upper part of figure 1(b). In the difference spectrum, two peaks are clearly exhibited, which are located at 0.90 and 3.21 eV higher in BE than the main peak, respectively. The photoemission spectrum of atomic Ni can be found in [24]. There are no atomic states related to the 0.90 eV peak. It is introduced merely due to the broadening of the peak for smaller clusters. The noticeable peak at 3.21 eV higher than the main peak confirms the existence of ^{3}F atomic state; with its variation arguing against a non-magnetic $3d^{10}$ final-state valence configuration. The Ni 6 eV satellite also originates from the triplet state (^{3}D and ^{3}P states) and shows some enhancement at small clusters, as shown in figure 1(b). However, since the 6 eV satellite is highly pronounced even for Ni bulk, the change observed here is weaker compared to the ^{3}F state. We then focus on the appearance of the 3.21 eV peak, which indicates that the ^{3}F atomic state changes with the dimension size. From here, we develop a way to illustrate the alternation of the Ni 3d population using the non-spin resolved photoemission method. On the other hand, the unfilled 3d states consist of part of the pure spin down states and part of the hybridized 3d–4sp states [7], which part would be filled first has not been indicated yet. The 3d–4sp unoccupied hybridized states are completely unpolarized, the filling of these states will generate singlet and triplet states evenly. The pure spin down states give rise only to the triplet states in photoemission spectra. Thus the drop in intensity of the ^{3}F state is an indication of the filling of 3d pure spin down states. The filling electron originally belongs to free-electron-like 4sp states, which are randomly polarized and highly overlapped with those 3d characters close to E_F. Thus, we conclude that the unfilled 3d pure spin down states is lower in energy and closer to E_F than those of the unfilled 3d–4sp hybridized states.

The results in figure 1 imply that the ^{3}F atomic state is likely to be modified upon annealing and Ar^+ ion irradiation. Through STM measurement, Tanner *et al* [15] have found that the Ni clusters annealed in UHV coarsened up to ∼880 K, but after this temperature the metal clusters did not grow any further. The agglomeration of Ni clusters upon annealing results in a broad d band and an increased 3d population. Figure 2(a) illustrates the Ni 2p XPS spectra for 5 min-deposited Ni clusters, together with those annealed at 100 and 200 °C for 5 min stepwise. To gain a better understanding of the spectra change, the comparison and difference between the as-deposited and the 200 °C annealed sample is shown in figure 2(b). Again, the peaks appearing at 0.91 and 3.25 eV higher than the main peak are attributed to the broadening of the peak and variation of the ^{3}F atomic state, respectively. From figure 2(a), the prominent drop at the feature B region should be noticed at 200 °C compared to the small fade at 100 °C. It is suggested that, if the feature B is caused by the oxidation process, the annealed clusters should present more. However, there is no evidence of this, as seen in figure 2. Another argument may be that metastable oxidation states of Ni exist at the interface between Ni and TiO_2 due to the fact that Ni may be associated with the interfacial oxygen, so the peak we assigned to the Ni ^{3}F atomic state may be due to an oxide-like environment from these interfacial atoms. The heats of formation per oxygen atom for NiO and Ni_2O_3 are −240.6 and −163.2 kJ mol^{-1}, respectively [25]. If there is any metastable oxidization state of Ni, it would be dominated by NiO rather than Ni_2O_3. We note that the chemical shift for Ni^{2+} and Ni^{3+} is 2.0 and 3.5 eV, respectively [35]. If the peak we assigned to the Ni ^{3}F atomic state is due to the oxidation state of Ni, it would be the metastable state of Ni^{3+}, which is less likely due to the above evidence. Thus, we eliminate the influence of oxidation process on the feature B. Imposing these results, we deduce that the evolution of feature B is free from the oxidation process but related to the variation of the ^{3}F states.

Thermal annealing triggers the agglomeration of the Ni clusters. The agglomeration of Ni clusters will make the 3d level electrons more populated, leading to a reduction of 3d hole number. As a result, the ^{3}F triplet state decreases upon annealing, as shown in figure 2. The parallel tendency of deposition-dose-based upturn of the cluster size denotes that filling up the 3d spin down unoccupied states is the intrinsic mechanism for populating the Ni 3d level when the cluster size is increased. The pronounced dip of the ^{3}F states at 200 °C is an indication that the Ni clusters become highly mobile on TiO_2(001) at this temperature. Based on these factors, we can modify the Ni 3d electron population easily by thermal annealing and gauge it by probing its 2p photoemission spectra.

In figures 1 and 2, revolution of the Ni 2p spectra demonstrate that the modified initial electronic structure of Ni clusters due to alteration of the Ni 3d minority electron population upon the cluster dimension is the origin of the variation of the ^{3}F triplet satellite state. This also implies that the initial electronic structure of the Ni cluster changes with dimension and can be probed by non-spin resolved photoemission through analysis of the ^{3}F triplet satellite state.

Besides the variation of the 3 eV satellite, the well-known Ni 6 eV satellite also exhibits different properties in reduced dimensional systems. Table 1 summarizes the angle resolved XPS (ARXPS) results performed on Ni foil. In table 1, the satellite intensity is evaluated as the ratio between satellite

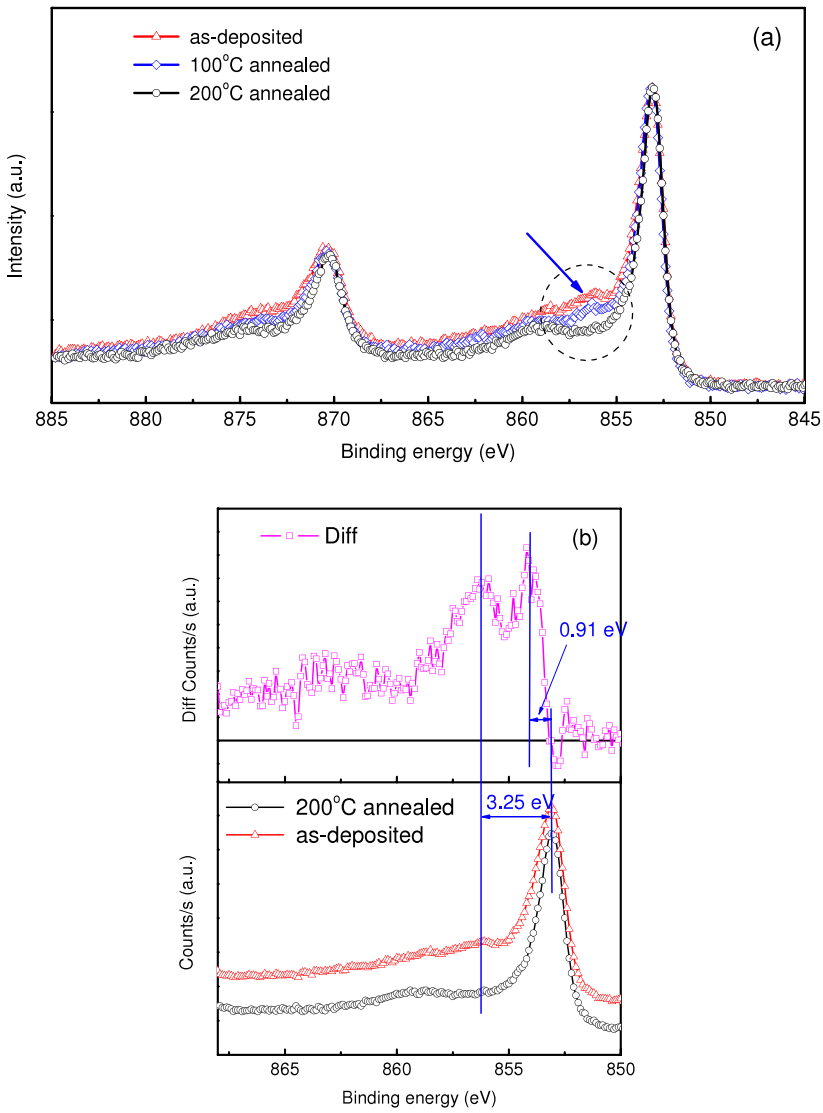

Figure 2. Ni $2p_{3/2}$ XPS spectra for 5 min-deposited Ni clusters annealed at 100 and 200 °C, respectively (a), annealing temperature is specified on the figure; the comparison (lower) and difference (upper) spectra between the as-deposited and 200 °C annealed spectra are shown in (b).

intensity (I_{sat}) and the main peak intensity (I_{main}). In this convention, the satellite intensity is doubled when detected at a take-off angle of 15° compared to normal detection (take-off angle of 90°). As we know, the spectra at low take-off angle carry more information from the surface, where the dimension is lower compared to bulk. By considering the inelastic mean free path of 1.26 nm [36], the probing thickness is about 0.98 nm at 15° take-off angle. For take-off angle of 40°, the probing thickness is 2.43 nm. In table 1, only a small increase is found for the ratio of satellite and main peak intensities when the take-off angle changes from 90° to 40°. This indicates that a notable enhancement of satellite intensity due to reduced dimension occurs only with a thickness less than 2.4 nm and most likely about 1.0 nm. The tendency that the satellite intensity increases with decreasing take-off angle is consistent with the current theoretical understanding of the origin of the 6 eV satellite [3, 4]. At the surface, the reduced atomic coordination leads to lattice contraction [37, 38] and hence increased Coulomb correlation energy U. The increased Coulomb correlation energy U and d–d electron correlation are the origin of the enhancement of satellite intensity. Since the Ni foil is in polycrystalline form, the orientation related band structure distribution can be ruled out as a reason for the variation of satellite intensity at different take-off angles.

Table 1. Ni 6 eV satellite intensity ratios with respect to the main peak for different take-off angles, together with the binding energies (BEs) and full width at half maximum (FWHM) of the main and the satellite peaks.

Take-off angle (deg)	BEs of main peak (FWHMs) (eV)	BEs of sat. peak (FWHMs) (eV)	I_{sat}/I_{main}
90	852.91 (0.92)	858.71 (3.03)	0.16
40	852.94 (0.93)	858.74 (3.26)	0.18
15	852.96 (0.98)	858.76 (4.04)	0.32

Apart from the cluster size, Ar^+ ion bombardment has the potential to control the shape of the nano-clusters [39]. The bombarded nano-clusters exhibit strong electronic size effects,

Table 2. The binding energy (BE) positions, differences, full width at half maximum (FWHM) and intensity ratios of Ni $2p_{3/2}$ main and satellite peaks for Ni foil, as-deposited and Ar^+ ion bombarded Ni clusters.

	BEs of main peak (FWHMs) (eV)	BEs of sat. peak (FWHMs) (eV)	Sat. energy (eV)	I_{sat}/I_{main}
Ni foil	852.91 (0.92)	858.71 (3.03)	5.80	0.16
As-deposited (30 min)	853.11 (1.00)	859.06 (2.73)	5.95	0.15
Ar^+ bombarded (60 s)	853.30 (1.18)	859.59 (2.96)	6.29	0.13

which are not related to the surface roughness and appear only on the supported clusters. Table 2 tabulates the 6 eV satellite energy and intensity ratio comparison of Ni foil, as-deposited clusters, and Ar^+ ion bombarded clusters. The corresponding Ni $2p_{3/2}$ spectra are shown in figure 3. Along with the induced electronic size effects, the shape of the Ni nano-clusters may be modified by Ar^+ ion bombardment. As reported for the Au/TiO_2 system [39], the sputtering modifies the cluster morphology from being a hemispherical island to being dot-like. As the Ar^+ ion bombardment produces nano-clusters and reduces both the lateral and vertical dimensions, quantum confinement is possible in either direction. As a result, we found the 6 eV satellite displays different properties upon Ar^+ ion bombardment. In this experiment, the bombardment is performed using 3 keV Ar^+ ions (current density $\sim 5\ \mu m^2$) with an incident angle of 53° with respect to the surface normal. Upon ion bombardment, the ^3F state does not change evidently. The large difference appears as a change of the 6 eV satellite energy, as shown in figure 3. In table 2, the bulk form Ni foil has the lowest satellite energy of 5.80 eV. The satellite energy is increased by 0.34 eV upon Ar^+ ion bombardment, together with a weak drop of satellite intensity, as shown in table 2. The variation of Ni 2p satellite energy is very interesting and has a potential use for diagnosis of the chemical environment of Ni atoms, and for the electronic structure of the Ni alloys [40]. This change may be related to the cluster shape change induced by Ar^+ ion bombardment as in Au/TiO_2. STM measurement would be helpful to gain more direct information about this interesting phenomenon.

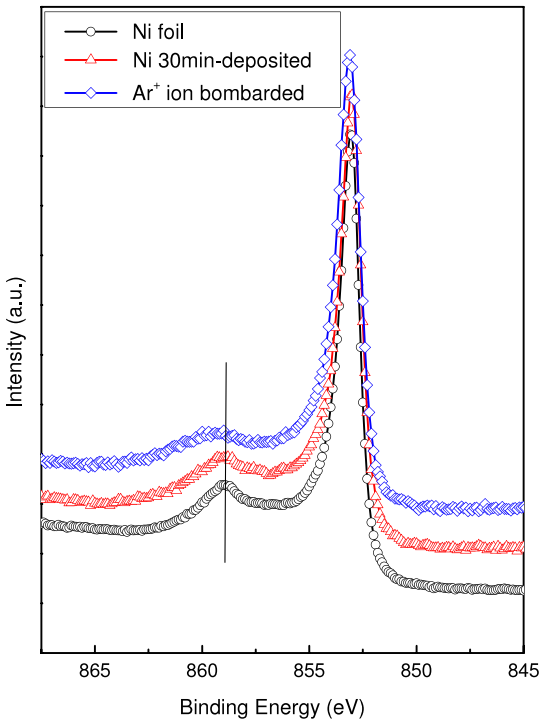

Figure 3. Ni $2p_{3/2}$ XPS spectra for Ni foil, 30 min-deposited Ni clusters, and after 20 s Ar^+ ion sputtering.

4. Conclusion

In conclusion, we used XPS to study the Ni 2p satellite of Ni clusters on TiO_2(001) as a function of Ni coverage as well as using annealing and Ar^+ ion bombardment. The variation of Ni 2p satellite with cluster size is discussed. The Ni 2p spectra results at low coverage confirm the existence of ^3F atomic states, with the variations arguing against a non-magnetic $3d^{10}$ final-state valence configuration. We demonstrate that the narrowed d band in the reduced dimensional clusters leads to intense ^3F triplet states in the Ni 2p spectra due to the lowered 3d electron population. The electrons in 4sp states prefer to transfer to unhybridized pure 3d spin down states, which are lower in energy than 3d–4sp hybridized states. Our results might be useful in terms of magnetic quantum dots or nanostructures to interpret their electronic structures. Due to the prominent change of the satellite features with low temperature annealing, it may be an efficient method to check other transition-metal systems where the satellite issue is still controversial. Here we suggest carrying out further theoretical calculations related to the Ni d–d interaction and the s–d hybridization for different sizes of Ni clusters on TiO_2(001), which would give more insight into this problem.

References

[1] Nath K G, Haruyama Y and Kinoshita T 2001 *Phys. Rev.* B **64** 245417
[2] Hüfner S 2003 *Photoelectron Spectroscopy: Principles and Applications* 3rd edn (Berlin: Springer)
[3] Clauberg R, Gudat W, Kisker E, Kuhlmann E and Rothberg G M 1981 *Phys. Rev. Lett.* **47** 1314
[4] Mårtensson N 1980 *Phys. Rev. Lett.* **45** 482
[5] Björneholm O, Andersen J N, Wigren C, Nilsson A, Nyholm R and Mårtensson N 1990 *Phys. Rev.* B **41** 10408
[6] Feldkamp L A and Davis L C 1979 *Phys. Rev. Lett.* **43** 151
[7] See A K and Klebanoff L E 1995 *Phys. Rev. Lett.* **74** 1454
[8] Sakisaka Y, Komeda T, Onchi M, Kato H, Masuda S and Yagi K 1987 *Phys. Rev.* B **36** 6383
[9] See A K and Klebanoff L E 1995 *Phys. Rev.* B **51** 11002
[10] Hövel H, Grimm B, Pollmann M and Reihl B 1998 *Phys. Rev. Lett.* **81** 4608

[11] Srivastava P, Haack N, Wende H, Chauvistré R and Baberschke K 1997 *Phys. Rev.* B **56** R4398
[12] Chen C 1990 *Phys. Rev. Lett.* **64** 2176
[13] Chen C 1993 *Phys. Rev.* B **48** 1318
[14] Binns C, Derbyshire H S, Bayliss S C and Norris C 1992 *Phys. Rev.* B **45** 460
[15] Tanner R E, Goldfarb I, Castell M R and Briggs G A D 2001 *Surf. Sci.* **486** 167
[16] Zhou J, Kang Y C and Chen D A 2003 *Surf. Sci.* **537** L429
[17] Tao J G, Pan J S, Huan C H A, Zhang Z, Cai J W and Wang S J 2008 *Surf. Sci.* **602** 2769
[18] Nesvizhskii A I, Ankudinov A L, Rehr J J and Baberschke K 2000 *Phys. Rev.* B **62** 15295
[19] Godehusen K, Richter T, Zimmermann P and Martins M 2002 *Phys. Rev. Lett.* **88** 217601
[20] Fujikawa K, Suzuki S, Koike Y, Chun W J and Asakura K 2006 *Surf. Sci.* **600** L117
[21] Clark E A, Yeske R and Birnbaum H K 1980 *Metall. Trans.* A **11** 1903–8
[22] Schelling P K, Yu N and Halley J W 1998 *Phys. Rev.* B **58** 1279
[23] Diebold U 2003 *Surf. Sci. Rep.* **48** 53–229
[24] Schmidt E, Schröder H, Sonntag B, Voss H and Wetzel H E 1983 *J. Phys. B: At. Mol. Phys.* **16** 2961
[25] Dean J A 1999 *Lange's Handbook of Chemistry* 15th edn (New York: McGraw-Hill)
[26] Czerwosz E, Dluzewski P, Kutner T and Stacewicz T 2003 *Thin Solid Films* **423** 161–8
[27] Fu Q and Wagner T 2005 *J. Phys. Chem.* B **109** 11697
[28] Fu Q, Wagner T, Olliges S and Carstanjen H D 2005 *J. Phys. Chem.* B **109** 944–51
[29] Fu Q and Wagner T 2007 *Surf. Sci. Rep.* **62** 431
[30] Hillebrecht F U, Fuggle J C, Bennett P A, Zołnierek Z and Freiburg C 1983 *Phys. Rev.* B **27** 2179
[31] Fuggle J C, Hillebrecht F U, Zeller R, Zołnierek Z, Bennett P A and Freiburg C 1983 *Phys. Rev.* B **27** 2145
[32] Kakizaki A 1998 *J. Electron Spectrosc. Relat. Phenom.* **88–91** 163
[33] Feldkamp L A and Davis L C 1980 *Phys. Rev.* B **22** 3644
[34] Amemiya K, Sakai E, Matsumura D, Abe H and Ohta T 2005 *Phys. Rev.* B **72** 201404
[35] Grosvenor A P, Biesinger M C, Smart R S and Mcintyre N S 2006 *Surf. Sci.* **600** 1771–9
[36] Soriano L, Preda I, Gutiérrez A, Palacín S, Abbate M and Vollmer A 2007 *Phys. Rev.* B **75** 233417
[37] Huang W J, Sun R, Tao J, Menard L D, Nuzzo R G and Zuo J M 2008 *Nat. Mater.* **7** 308–13
[38] Sun C Q 2004 *Phys. Rev.* B **69** 045105
[39] Karmakar P, Liu G F, Sroubek Z and Yarmoff J A 2007 *Phys. Rev. Lett.* **98** 215502
[40] Stadnik Z M, Fuggle J C, Miyazaki T and Stroink G 1987 *Phys. Rev.* B **35** 7400